Journal of Materials Chemistry A

Accepted Manuscript

ROYAL SOCIETY OF CHEMISTRY

www.rsc.org/materialsA

Journal Name

ARTICLE

A Self-powered System Based on Triboelectric Nanogenerator and Supercapacitor for Metal Corrosion Prevention

Received 00th January 20xx,
Accepted 00th January 20xx

DOI: 10.1039/x0xx00000x

www.rsc.org/

Xiaoyi Li,†[abc] Juan Tao,†[b] Wenxi Guo,[bd] Xiaojia Zhang,[b] Jianjun Luo,[b] Mengxiao Chen,[b] Caofeng Pan*[b] and Jing Zhu*[ac]

As water covers most of the earth's surface, energy of the ocean is abundant and almost unexplored, which can be one of the most environmentally friendly forms of energy. Prevention of metal corrosion plays an important role in national economic development and daily life. Here, we report a network of triboelectric nanogenerators (TENGs) and supercapacitors (SCs), which is also called the self-powered system, to harvest huge water energy for preventing metal corrosion. When TENG was integrated with SC, the output current is stable and continuous. The corrosion results indicate that the TENG-SC self-powered system can prevent about 80% degree of corrosion for Q235 steel in 0.5M NaCl solution. This work demonstrates the TENG-SC system, which is self-powered, flexible and environmentally friendly, can harvest and store large-scale blue energy from the ocean, and also rends an innovative approach toward preventing the metal corrosion without other power sources.

1. Introduction

Corrosion protection of metals plays an important role in national economic development and daily life.[1, 2] So far, tremendous efforts have been devoted to protecting the metals from corrosion and cathodic protection is considered as one of the most effective way.[3, 4] However, the traditional cathodic protection needs either a sacrificial anode or an external power source, which increases costs and limits its applications.[5] Therefore, constructing an integrated system which can easily harvest and store the renewable energy from the environment will rend an innovative and effective approach to prevent metal corrosion.

As water widely distributes across of the earth's surface, energy of the ocean is abundant, clean and renewable, which contributes to the sustainable development of human civilization. The blue energy from the ocean, which is less dependence on season, circadian rhythm, weather or temperature, has several advantages comparing with other renewable energies. Although numerous researches have been committed to harvesting the massive blue energy, the utilization of water wave energy needs to be further developed. Furthermore, the corrosion is more likely to take place for metals under the ocean environment condiction. Triboelectric nanogenerators (TENGs), which convert the mechanical energy to electricity, can solve the problem.[6-9]

Here, we report a network of triboelectric nanogenerators (TENGs) and supercapacitors (SCs), also called the self-powered system, to harvest huge water energy for preventing metal corrosion. The short-circuit current and open-circuit voltage of The TENG are 5 μA and 75 V. When integrated with SC, the output current of the device is stable and continuous. The corrosion results illustrate that the TENG-SC self-powered system can prevent about 80% degree of corrosion for Q235 steel in 0.5M NaCl solution. This technology provides an innovative and effective way to collect huge blue energy from the ocean and rends an original and effective approach to prevent the metal corrosion without other power sources. The concepts and works in this article can be used in a variety of applications and improve our living.

2. Experimental section

2.1 Fabricating and measurement of TENGs

A 30 μm-thick polytetrafluoroethylene (PTFE) film was adopted to be the friction material. After cleaned with alcohol and deionized water (DIW), the PTFE film was coated by a 10 nm thick Au film by magnetron sputtering (Discovery 635, Denton Vacuum). Then the film was etched by inductively coupled plasma (ICP) to create PTFE nanowires on the surface. Two copper electrodes (12cm*2cm) were deposited onto the back of the PTFE film by magnetic sputtering at 60 w for 30 min. Finally, the PTFE film with two copper electrodes was attached to a flexible acrylic substrate with the electrodes inside. And a pump (Jebao ECO) was used to generate water waves by controlling the movement of water to simulate the marine environment. The short-circuit current was measured by SR570 (Stanford Research System), and induced charge and open-circuit voltage were both tested by Keithley 6514 electrometer.

[a] National Center for Electron Microscopy in Beijing, School of Materials Science and Engineering, The State Key Laboratory of New Ceramics and Fine Processing, Key Laboratory of Advanced Materials (MOE), Tsinghua University, Beijing, China.
[b] Beijing Institute of Nanoenergy and Nanosystems, Chinese Academy of Sciences, Beijing, China.
[c] Center for Nano and Micro Mechanics, Tsinghua University, Beijing 100084, China.
[d] Research Institution for Biomimetics and Soft Matter and department of physics, Xiamen University, Xiamen, 361005, PR China
† Authors contributed equally to this work.
Electronic Supplementary Information (ESI) available: Figure S1-4. See DOI: 10.1039/x0xx00000x

2.2 Preparation of SCs

The highly flexible and transparent network electrodes for SCs were produced using electrospinning and sputtering method which was suggested by previous works.[10, 11] First of all, the 8 wt% polyvinyl butyral (PVB) alcohol solution was prepared at room temperature, and the PVB fibers were obtained by electrostatic spinning (TJ-8JNY) at the positive voltage 17 KV. Then, the PVB fibers were coated by a thin silver layer by magnetic sputtering at 100 w for 10 min and the core-shell fibers were immersed in DIW to dissolve the PVB. The Ag networks were then transferred to a polyethylene terephthalate (PET) substrate. The gel electrolyte of SCs was obtained by continuously adding PVA powder (25 g) and phosphoric acid (H_3PO_4, 20 g) into DIW (250 ml) at 90°C with stirring. Subsequently, PVA/H_3PO_4 gel electrolyte was spin-coated on PET/Ag network electrode at 1000r/min for 1 min. Finally, the cellulose acetate membrane was utilized as a separator.[12] Symmetrical electrodes were adopted to compose the SC in this study. The cyclic voltammetry (CV) curves were measured by SR570 with D345 and the galvanostatic charge/discharge (GCD) curves were tested by the Cell Testing System (LANHE). The autolab electrochemical workstation (Autolab, Eco-Chemie) was used to measure the open circuit potential.

3. Results and discussion

As our previous study, it has been demonstrated that water can be the power which can generate triboelectricity, and that the contact electrification between water and insulating polymer films has been used to harvest wave energy.[13-19] Figure 1 shows a schematic diagram and the output signals of the flexible TENG. Figure 1a illustrates the working principle of the TENG which harvests the water mechanical energy and converts it to electricity. When the PTFE thin film with two Cu electrodes at the backside is immersed into water, surface triboelectric charges arise at the water-PTFE interface. And because of the asymmetric surface charges, free electrons are induced to flow between two electrodes during the emerging and submerging process. The working mechanism of the TENG is shown in Figure S1. In order to enhance the output of the TENG, the PTFE surface is etched to create the nanowire arrays to increase the effective contact area. SEM image of the PTFE nanowire arrays is presented in Figure 1b. It can be found that the PTFE nanowires are uniformly distributed on the surface with an average diameter of 50nm. According to the previous work reported by Zhu et al., because of its uniform super hydrophobic property and considerable surface area, these nanowires play an important role in the process of harvesting water mechanical energy. In order to evaluate the electrical output performance of the TENG (100mm*42mm, shown in Figure S2b) with water, the short-circuit current (Fig. 1c), open-circuit voltage (Fig. 1d) and charge quantity (Fig. 1e) are measured when the TENG moves up and down in water. The peak of the current in Figure 1c is about 5 μA and the open-circuit voltage in Figure 1d can reach about 75 V. And the total amount of induced charges is about 30 nC in Figure 1e in one merging and submerging process. The electrical signals (including current, voltage and induced charges) increase when increasing the speed of the wave.[11] To develop a TENG network, thousands of TENGs are electrically connected in parallel to develop a network. And a pump is utilized to generate water waves by controlling the movement of water to simulate the marine environment. To reveal the law of the TENG networks for blue energy harvesting, three TENGs are fabricated into a small network (Figure S2a). Figure 1f demonstrates the output current of the small TENG network with unit number n=1, 2, 3 respectively. It is obvious that the current output increases when the unit number increases from 1 to 3.

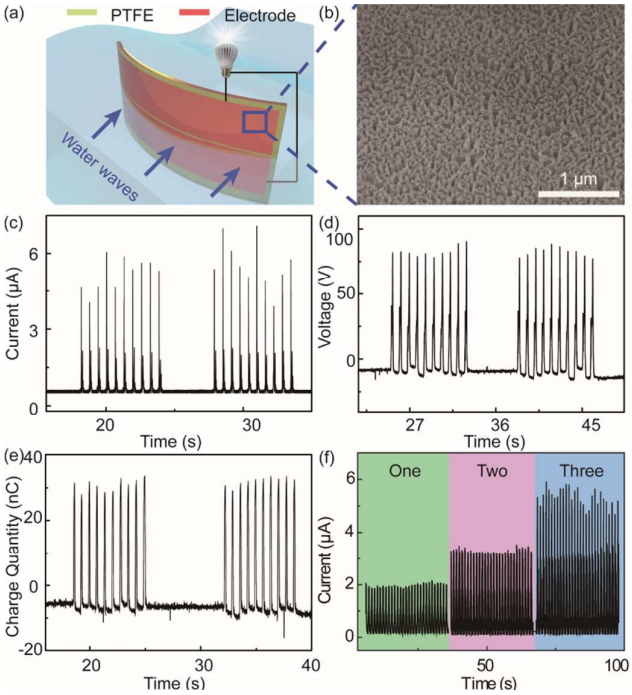

Figure 1. (a) Schematic diagram of the bent TENG in water waves. The up/down movement of the water surrounding the TENG induces electricity produced between the two electrodes. (b) SEM image of the polymer (PTFE) nanowires on the top surface of the polymer layer (PTFE). The short-circuit current (c), open-circuit voltage (d) and induced charges (e) of the TENG with the up and down movement in water. (f) The rectified short-circuit current of TENGs with unit number n=1, 2, 3.

Because the output signals of the TENG are pulsed and un-continuous, a flexible supercapacitor is designed to store the energy from the TENG and convent it to a more stable and continuous form. Figure 2a shows the schematic image of the flexible electrical double-layer supercapacitor with Ag network electrodes on PET substrate. The device consists of four components: the PET substrate, the Ag network electrodes, the solid electrolytes and a separator. The optical images of a typical SC in Figure 2b and 2c show that the SC is diaphanous and flexible with great potential in energy storage, flexible device and transparent electronic device.[20] The PVB network in

Figure 2d are fabricated by electrostatic spinning. After depositing Ag on the surface of the PVB fibers in Figure 2e, the obtained core-shell networks are immersed in DIW to remove the PVB. It can be observed that PVB networks are uniform intertwined, which enables network electrodes to present good conductivity after depositing metal Ag. The average diameter of the Ag fibers is about 3 μm and the convex surface is rough with nano structures (Figure S3), therefore the surface area of the electrodes can be remarkably enhanced. The micro and nano structures of materials increase the contact surface area between the electrode and the electrolyte.[21, 22] The cyclic voltammetry (CV) curves of flexible device with the scan rate ranging from 20 to 1000 mV s^{-1} are performed in the potential window of 0 to 0.8 V, as is shown in Figure 2e. These CV curves are found to be rectangular in shape within a selected range of potential even at high scan rates, indicating the fast diffusion of ions and a very rapid current response to voltage reversal in the active materials of electrodes. The CV curves in the potential window of 0 to 0.6 V, 0 to 0.8 V and 0 to 1 V with the same scan rate 500mV s^{-1} are shown in Figure 2f. The CV curves exhibit similar rectangular-like shapes even at a wide potential window, which indicates good rate capability, ideal supercapacitor behaviour and excellent stability of electrodes.[23, 24]

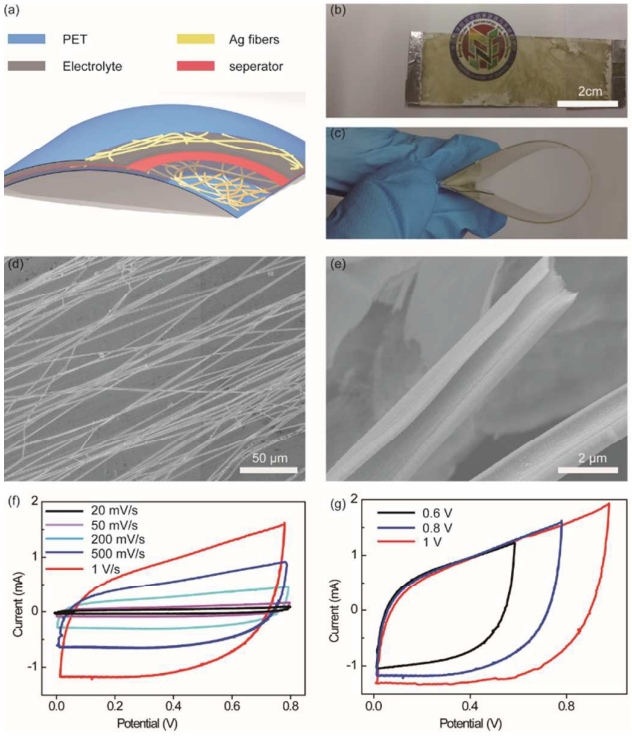

Figure 2. (a) Schematic of the flexible electrical double-layer supercapacitor (SC). Optical images of the diaphanous supercapacitor (b) and the flexible supercapacitor (c). SEM images of PVB fibers (d) and Ag fibers (e) by depositing Ag on the surface of PVB fibers and dissolving the PVB. (f) CV curves of the diaphanous flexible supercapacitor at different scan rates (20-1000 mV/s). (g) CV curves of the supercapacitor measured at different voltage windows.

Figure 3a shows the GCD curves of the supercapacitor at the different current values ranging from 5 to 50 μA. The GCD curves are similar in shape between 0 and 0.8 V and are nearly triangular shape in the charge-discharge cycles, which indicates that the supercapacitor can stably perform in various current values and also exhibit good symmetry.[25] The almost linear slopes at high discharge current values illustrate the electrochemical double layer behavior and further confirm the capacitive and fast charge/discharge properties of the supercapacitor.[21, 26, 27] According to GCD tests, the supercapacitor exhibits the highest capacitance of 1128 μF at a discharge current of 5 μA in Figure 3b. It can be seen that the capacitance decreases gradually and tends to be stable eventually with an increase in the current value from 5 to 50 μA, which can be attributed to progressively less efficient infiltration of ions into electrodes at higher scan rates.[28-30] At the lower current scan rates, the ions have sufficient time to gain access to diffuse from the electrolyte deep into electrodes. Nevertheless, there is no enough time for the irons to diffuse with the enhancement of scan rates, which causes the reduction of capacitance. The Ag network electrode with excellent electrical conductivity and high surface area can guarantee excellent capacitive behavior. The cycle stability is an important performance of SC when in practice. Figure 3c shows the long-term stability of the SC for 1000 cycles at a current of 50 μA. Interestingly, it can be observed that the discharge capacitance of the SC slightly increases and remains stable after 300 cycles. The electrolyte gradually penetrates into the hollow structure of the Ag network with the increasing of the effective interfacial area between the electrode and electrolyte, which causes the increasing in capacitance.[12] The inset in Figure 3c shows typical charge-discharge curves in a continuous operation for 30 cycles. In order to study the flexibility of the supercapacitor, the CV curves of the supercapacitor before and while being bent are performed under different bending angle. And no significant deviation of the CV curves is observed when the device is bended even to 150° in Figure 3d and 2b, indicating it possesses an excellent flexibility. The remarkable cycling stability, mechanical flexibility and capacitance retention of the flexible SC devices will be beneficial for their practical applications.

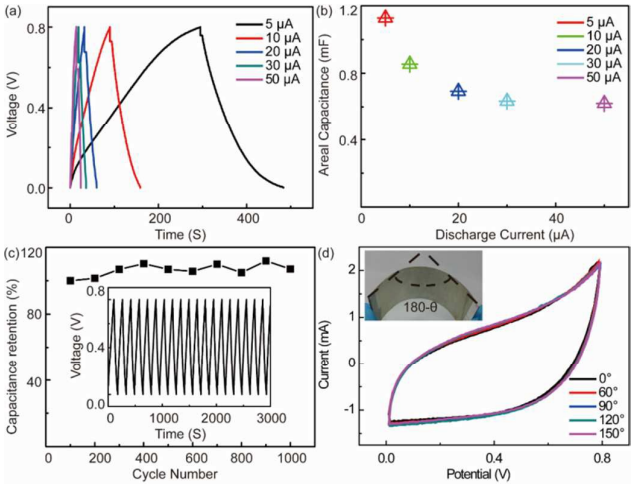

Figure 3. (a) Galvanostatic charge-discharge curves of the SC at the different current values ranging from 5 to 50 μA. (b) The capacitance under different discharge current. (c) Variation of capacitance stability of the SC with cycle number at the

current of 50 μA. The inset picture is the charge-discharge curves of the SC at 10 μA by 30 circles. (d) CV of the SC before bending (θ= 0°) and while being bent (θ= 60°, 90°, 120° and 150°).

To develop a TENG-SC network, thousands of TENG-SCs are electrically connected in parallel to develop a network for blue energy harvesting, as shown in Figure 4a. Figure 4b demonstrates the charge quantity of the SC powered by a TENG. When the TENG is turned on, a large quantity of charges are injected into the SC causing rapidly rise while the charge quantity stays stable when the TENG is off. In Figure 4c, the current of SC charged by TENG is the left part and discharging current of the SC with the external resistance of 100 KΩ is the right part. Since the output signals of the TENG are pulsed, the current flowing into the SC is also un-continuous as shown in the inset of Figure 4c. But when SC discharges with an external resistance of 100 KΩ, the output current is direct current and continuous, which is significant for its potential applications. The circuit diagram is shown in Figure S2c. This technology provides an innovative and effective method to collect huge blue energy from the ocean. And the energy stored in the SCs can be used for mental corrosion prevention,[8] replacing the batteries or powering the ocean environment monitoring sensors.

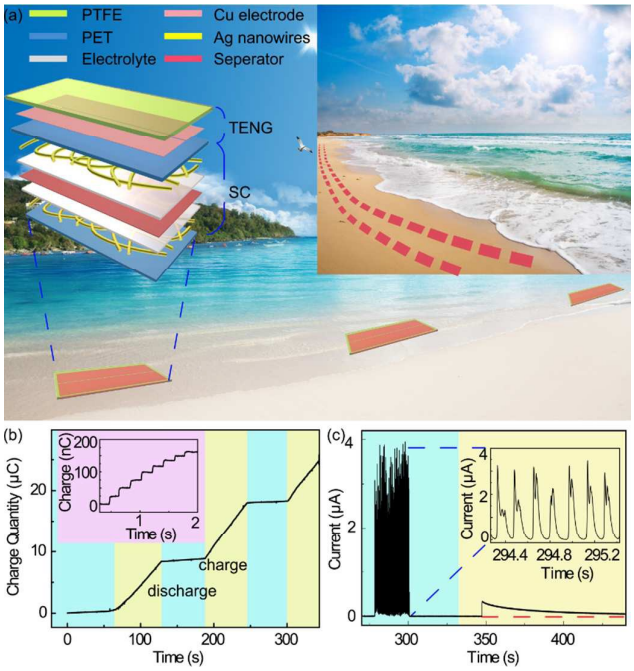

Figure 4. (a) Schematic illustration of the power pack (TENGs and SCs) networks which consist of thousands of single units on the beach. The power pack networks are built on the beach to harvest the wave energy and storage the electric energy. (b)The charge quantity of the supercapacitor charged by TENG. (c) The current of SC charged by TENG and discharging current of the SC with the external resistance of 100 KΩ. The SC converts the pulsed current generated by TENG to a stable and continuous signal.

The energy generated from the TENG and stored in the SC can be used in a variety of applications and improve our living. Figure 5a shows the structures and working principle of the TENG-SC cathodic protection system. When the TENGs start to harvest the mechanical energy of the water wave (0.2m/s, 1Hz), the transferred electrons will be injected into the protected steels, resulting in a cathodic polarization. Figure 5b indicates the open circuit potential of 403SS steel electrode immersed in 0.5 M NaCl solution. When the TENG-SC system is not working, the potential of the steel electrode is about -0.35 V. It exhibits a drastically negative shift to -0.6 V when the TENG is turned on as the green part in Figure 5b, indicating the steel become more stable with the help of the SC. It is worth to note that when the TENG is turned off, the potential will not recover to its original value quickly but stays at another platform at about -0.5 V for a while, as shown in the purple part of Figure 5b.

Finally the weight-loss tests for Q235 carbon steels are also carried out to further evaluate the corrosion protection capacity of our TENG-SC cathodic protection system. The optical images of the surface morphology of the Q235 carbon steels with and without TENG-SC self-powered system for different time are shown in Figure 5c. It is obvious that the steel without TENG-SC has much more red rust on the surface than that with TENG-SC after 1-2 h of immersion. Generally once the corrosion spots appear on the surface of the steel, the corrosion rate increases quickly and a large quantity of rust expands on the surface. After 6h of immersion in the 0.5M NaCl solution, a thick film of rust covers on the surface of steel without TENG-SC, while still only a few corrosion spots remains on the steel with TENG-SC. The results greatly prove that the TENG-SC self-powered system can effectively reduce the corrosion rate. Furthermore, SEM images of the steels with and without TENG-SC are shown in Figure S4, which also indicates that the TENG-SC self-powered system can prevent metal corrosion signally. It has been proved in our previous work that the open circuit potential of the steel decreases when the external solution resistance increases.[8] The weight-loss tests demonstrate that the TENG-SC self-powered system can prevent about 80% degree of corrosion for Q235 steel in 0.5M NaCl solution when the external resistance is 0.2 MΩ.

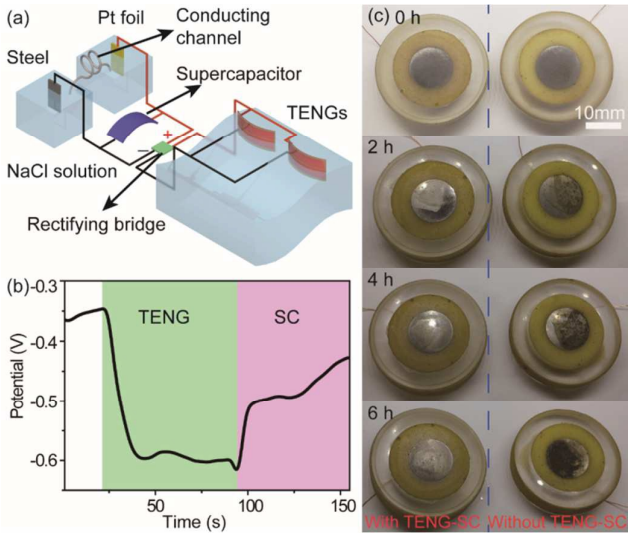

Figure 5. (a) The structures and working principle of the TENG-SC cathodic protection system. (b) The open circuit potential changes of a pure 403SS electrode coupled with and without the power pack. (c) The digital photographs of the surface morphology of Q235 carbon steels after immersing in 0.5 M NaCl solution for different time. The Q235 specimens were separated into two groups; one group specimens (on the left) were coupled to the negative pole of three power packs while the others (on the right) were not.

Conclusions

We report a network of TENGs and SCs, which is also called the self-powered system, to harvest huge water energy for preventing metal corrosion. The TENG delivers a short-circuit current of 5 μA and open-circuit voltage of 75 V. When integrated with SC, the output current of the device is stable and continuous. The corrosion results illustrate that the TENG-SC self-powered system can prevent about 80% degree of corrosion for Q235 steel in 0.5M NaCl solution. With the high sensitivity to water waves, the TENG-SC self-powered system can not only be used in strong wave circumstances (ocean) but also applied in many other conditions, such as lake, river and swimming pool. This technology provides a self-powered, flexible, extremely cost-effective, lightweight, environmentally friendly and easily implemented system to harvest huge blue energy from the ocean. In addition, our TENG-SC can be integrated with solar cells or wind energy collectors to harvest various kinds of energies,[31] which can be immediately adopted in a variety of applications, such as preventing the metal corrosion,[32] replacing the batteries and powering the ocean environment monitoring sensor.

Acknowledgements

This work was financially supported by the "thousands talents" program for pioneer researcher and his innovation team, China; National 973 Project of China (2015CB654902); Chinese National Natural Science Foundation (11374174，51390471); President Funding of the Chinese Academy of Sciences; National Natural Science Foundation of China (No.51272238, 21321062, 51432005 and 61405040); Beijing City Committee of science and technology (Z131100006013004, Z131100006013005). This work made use of the resources of the National Center for Electron Microscopy in Beijing and Beijing Institute of Nanoenergy and Nanosystems, Chinese Academy of Sciences.

Notes and references

1. C. Punckt, M. Bolscher, H. H. Rotermund, A. S. Mikhailov, L. Organ, N. Budiansky, J. R. Scully and J. L. Hudson, *Science*, 2004, **305**, 1133-1136.
2. H. Park, K. Y. Kim and W. Choi, *Chem. Commun.*, 2001, 281-282.
3. M. M. S. Cheung and C. Cao, *Constr. Build. Mater.*, 2013, **45**, 199-207.
4. J. Xu and W. Yao, *Constr. Build. Mater.*, 2009, **23**, 2220-2226.
5. S. Yehia and J. Host, *ACI Mater.*, 2010, **107**, 577-585.
6. C. F. Pan, Z. T. Li, W. X. Guo, J. Zhu and Z. L. Wang, *Angew. Chem., Int. Ed.*, 2011, **50**, 11192-11196.
7. S. Wang, L. Lin and Z. L. Wang, *Nano Lett.*, 2012, **12**, 6339-6346.
8. W. X. Guo, X. Y. Li, M. X. Chen, L. Xu, L. Dong, X. Cao, W. Tang, J. Zhu, C. J. Lin, C. F. Pan and Z. L. Wang, *Adv. Funct. Mater.*, 2014, **24**, 6691-6699.
9. S. Wang, L. Lin, Y. Xie, Q. Jing, S. Niu and Z. L. Wang, *Nano Lett.*, 2013, **13**, 2226-2233.
10. H. Wu, D. S. Kong, Z. C. Ruan, P. C. Hsu, S. Wang, Z. F. Yu, T. J. Carney, L. B. Hu, S. H. Fan and Y. Cui, *Nat. Nanotech.*, 2013, **8**, 421-425.
11. W. X. Guo, X. J. Zhang, R. M. Yu, M. L. Que, Z. M. Zhang, Z. W. Wang, Q. L. Hua, C. F. Wang, Z. L. Wang and C. F. Pan, *Adv. Energy Mater.*, 2015, **5**, 1500141.
12. S. H. Li, D. K. Huang, B. Y. Zhang, X. B. Xu, M. K. Wang, G. Yang and Y. Shen, *Adv. Energy Mater.*, 2014, **4**, 1301655.
13. G. Zhu, Y. J. Su, P. Bai, J. Chen, Q. S. Jing, W. Q. Yang and Z. L. Wang, *Acs Nano*, 2014, **8**, 6031-6037.
14. Z. H. Lin, G. Cheng, S. Lee, K. C. Pradel and Z. L. Wang, *Adv. Mater.*, 2014, **26**, 4690-4696.
15. Z. H. Lin, G. Cheng, L. Lin, S. Lee and Z. L. Wang, *Angew. Chem., Int. Ed.*, 2013, **52**, 12545-12549.
16. Z. H. Lin, G. Cheng, W. Z. Wu, K. C. Pradel and Z. L. Wang, *Acs Nano*, 2014, **8**, 6440-6448.
17. M. X. Chen, X. Y. Li, L. Lin, W. M. Du, X. Han, J. Zhu, C. F. Pan and Z. L. Wang, *Adv. Funct. Mater.*, 2014, **24**, 5059-5066.
18. J. Chen, J. Yang, Z. L. Li, X. Fan, Y. L. Zi, Q. S. Jing, H. Y. Guo, Z. Wen, K. C. Pradel, S. M. Niu and Z. L. Wang, *Acs Nano*, 2015, **9**, 3324-3331.
19. G. Cheng, Z. H. Lin, Z. L. Du and Z. L. Wang, *Acs Nano*, 2014, **8**, 1932-1939.
20. Y. Hou, L. Y. Chen, P. Liu, J. L. Kang, T. Fujita and M. W. Chen, *J. Mater. Chem. A*, 2014, **2**, 10910-10916.
21. X. L. Chen, H. J. Lin, J. Deng, Y. Zhang, X. M. Sun, P. N. Chen, X. Fang, Z. T. Zhang, G. Z. Guan and H. S. Peng, *Adv. Mater.*, 2014, **26**, 8126-8132.
22. B. Y. Ahn, E. B. Duoss, M. J. Motala, X. Y. Guo, S. I. Park, Y. J. Xiong, J. Yoon, R. G. Nuzzo, J. A. Rogers and J. A. Lewis, *Science*, 2009, **323**, 1590-1593.

23. K. Y. Xie and B. Q. Wei, *Adv. Mater.*, 2014, **26**, 3592-3617.
24. X. F. Wang, X. H. Lu, B. Liu, D. Chen, Y. X. Tong and G. Z. Shen, *Adv. Mater.*, 2014, **26**, 4763-4782.
25. L. B. Hu, H. Wu, F. La Mantia, Y. A. Yang and Y. Cui, *Acs Nano*, 2010, **4**, 5843-5848.
26. Z. Zheng, J. J. Chen, R. Yoshida, X. Gao, K. Tarr, Y. H. Ikuhara and W. L. Zhou, *Nanotechnology*, 2014, **25**, 435406.
27. Z. Niu, L. Zhang, L. Liu, B. Zhu, H. Dong and X. Chen, *Adv. Mater.*, 2013, **25**, 4035-4042.
28. S. J. He and W. Chen, *Nanoscale*, 2015, **7**, 6957-6990.
29. Z. J. Su, C. Yang, B. H. Xie, Z. Y. Lin, Z. X. Zhang, J. P. Liu, B. H. Li, F. Y. Kang and C. P. Wong, *Energy Environ. Sci.*, 2014, **7**, 2652-2659.
30. F. Zhang, T. F. Zhang, X. Yang, L. Zhang, K. Leng, Y. Huang and Y. S. Chen, *Energy Environ. Sci.*, 2013, **6**, 1623-1632.
31. X. B. Xu, S. H. Li, H. Zhang, Y. Shen, S. M. Zakeeruddin, M. Graetzel, Y. B. Cheng and M. K. Wang, *Acs Nano*, 2015, **9**, 1782-1787.
32. X. J. Zhao, G. Zhu, Y. J. Fan, H. Y. Li and Z. L. Wang, *Acs Nano*, 2015, **9**, 7671-7677.